DOI: 10.1002/fuce.201000082





# Study of Methanol-tolerant Oxygen Reduction Reaction at Pt–Bi/C Bimetallic Nanostructured Catalysts

A. M. Remona[1]*, and K. L. N. Phani[2]

[1] Department of Chemistry, Fatima College, Madurai – 625 018, Tamil Nadu, India
[2] EEC Division, Central Electrochemical Research Institute, Karaikudi – 630 006, Tamil Nadu, India

Received May 01, 2010; accepted December 26, 2010

## Abstract

The nanostructured platinum–bismuth catalysts supported on carbon ($Pt_3Bi/C$, PtBi/C and $PtBi_3/C$) were synthesised by reducing the aqueous metal ions using sodium borohydride ($NaBH_4$) in presence of a microemulsion. The amount of metal loading on carbon support was found to be 10 wt.-%. The catalyst materials were characterised by X-ray diffraction (XRD), X-ray fluorescence (XRF), transmission electron microscope (TEM) and electroanalytical techniques. The $Pt_3Bi/C$, PtBi/C and $PtBi_3/C$ catalysts showed higher methanol tolerance, catalytic activity for oxygen reduction reaction (ORR) than Pt/C of same metal loading. The electrochemical stability of these nano-sized catalyst materials for methanol tolerance was investigated by repetitive cycling in the potential range of –250 to 150 $mV_{MSE}$. Bi presents an interesting system to have a control over the activity of the surface for MOR and ORR. All Pt–Bi/C catalysts exhibited higher mass activities for oxygen reduction (1–1.5 times) than Pt/C. It was found that PtBi/C catalyst exhibits better methanol-tolerance than the other catalysts.

**Keywords:** Methanol-tolerance, Microemulsion, Nanocatalyst, Oxygen Reduction, Pt–Bi alloy.

## 1 Introduction

The oxygen reduction reaction (ORR) is an important cathode reaction in direct methanol fuel cells (DMFCs). Platinum is a widely used as electrocatalyst for ORR due to its high catalytic activity and excellent stability [1]. The ORR occurs by the proton and electron transfer to the oxygen or hydroxide, which are strongly adsorbed on the platinum surface at an electrode potential where the overall reaction is at equilibrium [2, 3]. The density functional theory calculations of Norskov et al. for ORR [3] resulted a volcano-shaped relationship between the rate of the cathode reaction and the oxygen adsorption energy. This model envisages that Pt is the best cathode material and the alloying of the platinum with other metals can be used to improve the cell performance.

Platinum is also the most active metal for methanol oxidation reaction (MOR), but it is well-known that it is readily poisoned by carbon monoxide species, which are strongly adsorbed on platinum active sites at room or moderate temperatures. The ORR in a polymer electrolyte membrane fuel cell (PEMFC) is generally affected by the methanol crossover from anode to the cathode compartment, results the cathodic overpotential losses in the range of 0.3–0.4 V [4, 5]. An imperative solution to this phenomenon is to develop new electrode catalysts with both higher methanol-tolerance and oxygen reduction activity than Pt.

The non-noble metal electrocatalysts such as ruthenium chalcogenide catalysts [6, 7] and transition metals attached to macrocyclic ligands [8, 9] showed promising methanol-tolerance but their oxygen reduction capabilities are inferior to Pt. Hence, in recent years, interest in the research of non/low-Pt-content methanol-tolerant catalysts has been renewed, driven by the cost reduction and reliability in the development of PEMFC systems [3, 5, 10–18]. The increase in catalytic performance of the catalysts is accounted by the change in Pt–Pt distance [15], increase in *d*-band vacancies [17], surface roughening [13] and the relative effects on the surface adsorbed OH species [18]. Investigations have been made to

[*] *Corresponding author, mremona@yahoo.com*

understand the reasons behind the improved performance of Pt-based bimetal catalysts where the second metal may be Fe, Co, Ni, Cu or Cr [5, 10–13, 19]. Though there was significant improvement in ORR, the exact reaction occurring at the bimetallic catalysts remains elusive.

The commonly employed second metals in many Pt-based bimetal catalysts for oxygen reduction are first row transition metals such as chromium, iron, nickel, palladium, cobalt, etc. However, a metalloid like bismuth, in the form of an alloy with Pt can exhibit an increase in catalytic activity for oxygen reduction in comparison with pure Pt. Reports are available for bismuth-based electrocatalysts for ORRs such as gold–bismuth [20, 21] and platinum–bismuth bimetal catalysts [10, 22–26]. However, most of the oxygen reduction studies using bismuth-incorporated bi- or tri-metal catalysts cited in the literature was executed in alkaline medium. Hence, there is an interest in Pt–Bi/C catalysts for ORR in acid electrolytes. Moreover, the studies available for Pt–Bi catalyst for ORR are inadequate and a complete analysis of the composition effect of Pt–Bi catalyst is yet to be established. From this viewpoint, the work was framed to investigate the composition effect of the platinum and bismuth for oxygen reduction and to ascertain a Pt–Bi catalyst, which can exhibit highest catalytic activity.

The present study comprises the synthesis of three Pt–Bi/C bimetal catalysts of different compositions such as $Pt_3Bi/C$, PtBi/C and $PtBi_3/C$ by varying Pt/Bi atomic ratios using a microemulsion method. The catalysts materials were characterised by X-ray fluorescence (XRF), X-ray diffraction (XRD) and transmission electron microscope (TEM) techniques and electrochemical methods. All the three Pt–Bi/C catalysts were found to be methanol-tolerant. The ORR studies were performed in 0.5 M sulphuric acid, saturated with oxygen both in the presence and absence of methanol using a rotating disc electrode.

## 2 Experimental

### 2.1 Synthesis of Catalyst Materials

The catalyst materials were synthesised by a microemulsion method. The microemulsion was prepared by mixing Triton X-100 (10%), cyclohexane (35%) and 2-propanol (40%) as reported by Zhang and Chan [27]. An aqueous solution of chloroplatinic acid ($H_2PtCl_6{\cdot}6H_2O$) (15%) was mixed with the microemulsion. The reducing agent, an aqueous solution of sodium borohydride (stoichiometrically excess) was mixed with another microemulsion mixture of same composition. The microemulsions containing metal and the reducing agent were mixed together with continuous stirring. The catalysts support used in the study is Vulcan XC 72R (commercially available carbon powder with the specific surface area of 250 $m^2\ g^{-1}$). The required amount of carbon was added in the form of slurry into the reaction vessel. The stirring was continued for about 8 h for the adsorption of platinum nanoparticles on carbon. After ensuring the complete reduction of platinum on carbon matrix by analysing the solution for the presence of platinum by atomic absorption spectroscopy (AAS), the Pt nanoparticles adsorbed on carbon were separated by ultracentrifugation, washed several times with millipore water and acetone to remove the surfactant completely and dried in a vacuum desiccator.

For the preparation of other Pt–Bi/C catalysts appropriate concentrations of chloroplatinic acid and bismuth nitrate were used to obtain the stoichiometries of $Pt_3Bi/C$, PtBi/C and $PtBi_3/C$. The metal loading in all the Pt–Bi/C catalysts including Pt/C was 10 at. wt.-%. Table 1 displays the expected and actual atomic compositions of the bimetal catalysts obtained from XRF studies. The values are agreed with atomic compositions of the individual metals in the bimetal catalysts.

### 2.2 Characterisation of the Catalyst Materials

The atomic ratio of platinum and bismuth in Pt–Bi/C catalysts was determined by XRF technique using Horiba X-ray analytical microscope XGT – 2700. X-ray diffraction patterns of the catalysts were obtained from STOE X-ray diffractometer in Bragg–Brentano geometry using $CuK_\alpha$ radiation ($\lambda$ = 1.5406 Å). The XRD patterns were recorded in the $2\theta$ value between 20° and 100° with the scan rate of 2 $min^{-1}$. The particle sizes were determined using CM200 super power STEM. For TEM analysis, the samples were dispersed well in 2-propanol and dispensed directly onto the sample grit.

### 2.3 Electrode Preparation

The electrodes used in this work were the nanostructured catalysts loaded electrode as working electrode, Pt foil and mercury-mercurous sulphate electrodes (MSE) as counter and reference electrodes, respectively. The electrolyte used was 0.5 M sulphuric acid.

The preparation of rotating disc working electrode (RDE) for electro-reduction of oxygen is as follows: prior to catalyst loading, a rotating disc glassy carbon electrode with diameter of 0.5 cm is polished using 0.2 μm alumina slurry and then washed well in deioniser water and cleaned ultrasonically to remove any impurities present on the surface. About 10 mg of the catalyst was ultrasonically dispersed in 1 mL of dis-

Table 1 Structural parameters of the Pt/C and Pt–Bi/C catalysts.

| Catalysts | Ratio of atomic wt.-% of Pt and Bi | Stoichiometry | Crystalline size (nm) | EASA ($m^2\ g^{-1}$) |
|---|---|---|---|---|
| Pt/C | 100 | Pt/C | 3.4 | 76.2 |
| $Pt_3Bi/C$ | 73.87:26.13 | $Pt_{2.83}Bi/C$ | 2.8 | 67.0 |
| PtBi/C | 52.83:47.17 | $Pt_{1.12}Bi/C$ | 2.7 | 24.0 |
| $PtBi_3/C$ | 25.15:74.85 | $PtBi_{2.97}/C$ | 2.9 | 14.3 |

Stoichiometry values are obtained from XRF studies. Crystallite sizes are determined from TEM analysis. EASA values are derived from the $Q_H$ values.

  

tilled water and 100 mg of 5% w/w Nafion®(117) (Fluka) in an ultrasonicator bath for 30 min. This solution is termed as catalyst ink. A 10 µL catalyst ink was dispensed onto the RDE and the electrode was used after drying. The electrode was coupled with pine rotator assembly for ORR studies.

All the other electrochemical studies were done using a film of the synthesised catalyst casted on polycrystalline Au disc electrode (diameter – 1.6 mm) as working electrode. The volume of the catalysts link dispensed on polycrystalline gold electrode was 2 µL. The cyclic voltammograms (CVs) of the catalysts were recorded in 0.5 M sulphuric acid and the methanol oxidation studies were conducted in 0.5 M sulphuric acid containing methanol.

The potential of the working electrodes was controlled by using a PGSTAT-30 AUTOLAB system. The current values were normalised with respect to geometrical area of the electrode and plotted as current densities.

## 3 Results and Discussion

### 3.1 XRD Studies

The XRD patterns of the catalysts are presented in Figure 1. All the carbon-supported catalysts show *fcc* crystalline structure. In all the patterns, a broad peak seen around $2\theta \sim 25°$ is due to the [002] plane of the hexagonal structure of Vulcan XC-72R, which acts as catalyst support. The XRD patterns of Pt/C show four Bragg peaks due to [111], [200], [220] and [311] indicating *fcc* phase with the space group of *Fm3m*. The lattice parameter ($a_o$) for Pt/C is 0.3926 ± 0.00182 nm.

The XRD patterns of $Pt_3Bi/C$ mainly resemble Pt/C showing the single-phase disordered structure (solid solution). The four diffraction peaks of $Pt_3Bi/C$ bimetallic catalyst are slightly shifted to lower $2\theta$ values with respect to the corresponding peak of Pt/C. The shift of the peaks to lower angles reveals the alloy formation between Pt and Bi, which is caused by the incorporation of Bi in the *fcc* structure. The lattice constant for the $Pt_3Bi/C$ catalyst is 0.3906 ± 0.00163 nm.

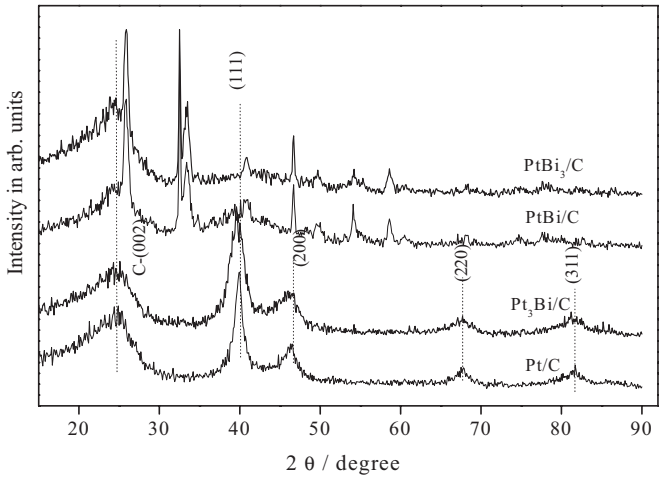


Fig. 1 XRD patterns of the Pt/C and Pt–Bi/C catalysts.

However, the catalysts with relatively high bismuth loading viz., PtBi/C and $PtBi_3/C$ catalysts exhibit different XRD patterns when compared with $Pt_3Bi/C$. The reflections observed for these two catalysts show the characteristic features of Pt and also the presence of non-alloyed Bi, which may be in the oxide form. The peaks at $2\theta$ values 46.8° and 48.7° correspond to rhombohedral structure of Bi [28, 29]. Peak broadening suggests smaller particle size. The other reflections with smaller intensity can be indexed to BiO, $Bi_2O_3$, etc. The peaks of Pt–Bi/C catalysts are broader than those of Pt/C, which indicate the increase in surface area of these catalyst materials. As the bismuth loading increases, the peak intensities are reduced.

### 3.2 TEM Characterisation

Figure 2 shows the TEM images of Pt/C, $Pt_3Bi/C$, PtBi/C and $PtBi_3/C$ catalysts and their corresponding particle size distribution histograms based on the observation of more than 400 nanoparticles. From the figure, it is understood that the nanoparticles of Pt/C and alloy catalysts are well distributed on the surface of the carbon support. The mean particle diameter of Pt/C is 3.4 nm. The catalyst with relatively low Bi contents ($Pt_3Bi/C$) yields non-homogeneous distribution of particles with a mean particle diameter of 2.9 nm. Whereas in the PtBi/C and $PtBi_3/C$ catalysts, the distribution is quite wide and the mean particle diameters of these catalysts are 4.7 and 7.4 nm, respectively. Though the same method is adopted for the synthesis, a variation in the particle size is due to the agglomeration of the particles.

The XRF, XRD and TEM characterisations show the method adopted for the synthesis yields nanostructured catalysts with narrow particle size having expected compositions and distributed well on the carbon matrix.

### 3.3 Electrochemical Characterisation

CVs of the Pt/C and Pt–Bi/C catalysts in 0.5 M $H_2SO_4$ medium are shown in Figure 3. The CVs were recorded in the potential region of –650 to 700 $mV_{MSE}$ at a sweep rate, 50 mV $s^{-1}$. Pt/C shows hydrogen adsorption/desorption peaks and pre-oxidation/reduction peaks in the potential window of –650 to –450 $mV_{MS}$. However, no well-defined hydrogen adsorption/desorption peaks are observed for all these catalysts, suggesting the high dispersion of the catalysts with disordered surface structure. The electrochemical active surface area (EASA) values for Pt–Bi/C catalysts are lower than that of Pt/C. The larger EASA value of Pt/C catalyst might be due to the dissolution of hydrogen into bulk Pt/C catalyst. However, for the Pt–Bi/C catalysts, the dissolution into bulk Pt–Bi/C might be restrained by the existence of bismuth. The EASA values of the catalysts estimated using the reported procedure [30] are listed in Table 1.

For Pt–Bi/C catalysts, the area under the hydrogen adsorption and desorption peaks are lower than that of Pt/C. This is due to the decrease in the number of platinum active

  

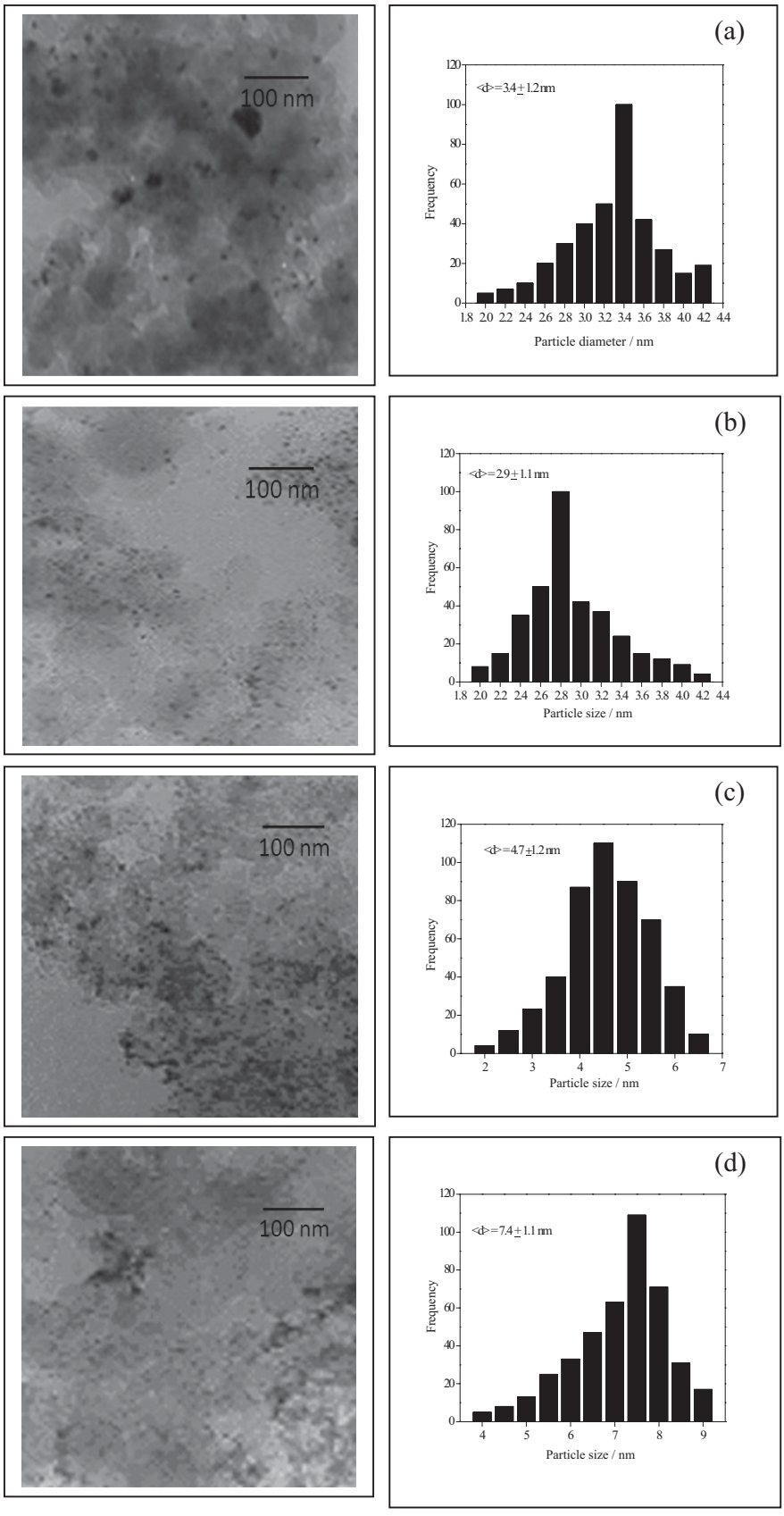


Fig. 2 TEM images of (a) Pt/C, (b) $Pt_3Bi/C$, (c) PtBi and (d) $PtBi_3/C$ catalysts with 10 wt.-% metal loading along with the corresponding particle size distribution histograms.

sites with an increasing amount of bismuth. The oxidation of PtBi/C and $Pt_3Bi/C$ catalysts occur at more negative (cathodic) potentials by 83 and 64 $mV_{MSE}$, respectively, than that of Pt/C except $PtBi_3/C$. Whereas $PtBi_3/C$ catalyst is showing the surface oxidation peak at more anodic values i.e. 178 $mV_{MSE}$ more positive from that of Pt/C.

Figure 4 compares the CVs of Pt/C, $Pt_3Bi/C$, PtBi/C and $PtBi_3/C$ catalysts both in the presence and absence of 0.5 M methanol under similar experimental conditions. Pt/C shows well-defined methanol oxidation profiles. The CVs of Pt–Bi/C catalysts recorded both in presence and absence of methanol appears qualitatively similar indicating the resistance of these catalysts to methanol electrosorption. In addition, the hydrogen adsorption charges ($Q_H$) of Pt–Bi/C catalysts are not affected in the presence of methanol. A minor blocking of the hydrogen adsorption is observed for $Pt_3Bi/C$, but there is no noticeable increment in the current values in methanol oxidation region (–250 to 500 $mV_{MSE}$). However, for $PtBi_3/C$ catalyst, the CV obtained in presence of methanol is decreased when compared with the CV recorded in the absence of methanol and the reason for this behaviour could not be commented.

It is important to note that at all Bi composition; the catalysts display resistance to methanol oxidation. The adsorption of methanol on the surface of Pt–Bi/C catalysts does not occur and the reasons are discussed later in this section. Also it is stated in the literature, the Pt–Bi catalysts is also virtually immune to CO poisoning when treated with carbon monoxide due to the geometric effects [31, 32] and hence this geometric effect may be the prime reason for the methanol-resistance behaviour of the Pt–Bi/C catalysts. An important drawback of bismuth in bimetal catalysts is that it suffers from leaching of bismuth into the solution on anodic potential treatments [33, 34].

To find the methanol tolerance level of the Pt–Bi/C catalysts, the experiments were performed by varying methanol concentration from 0.1 to 1.5 M and the

  

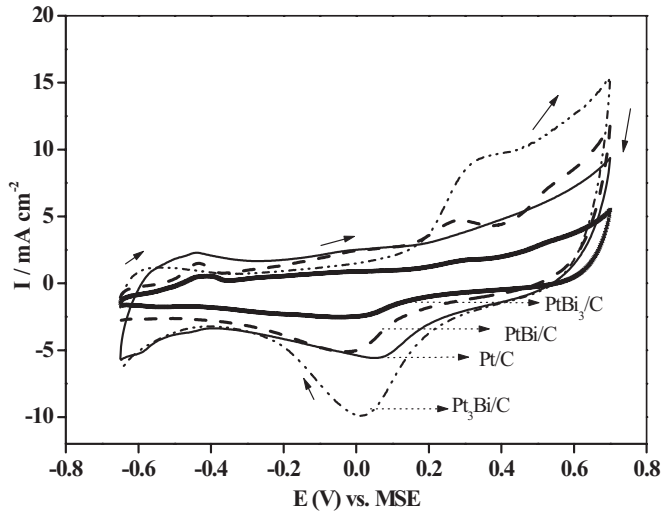


Fig. 3 Cyclic voltammograms of the Pt/C catalyst and Pt–Bi/C catalysts in 0.5 M $H_2SO_4$ at 50 mV $s^{-1}$ in the potential range of –650 to 700 $mV_{MSE}$ (current densities are normalised to the geometric surface area).

subsequent increase in methanol concentration do not result methanol oxidation in the potential range of –250–150 $mV_{MSE}$. As observed from the literature, the high anodic treatment of Pt–Bi/C catalysts causes leaching of bismuth from the catalyst surface and if that happens to the catalysts used in this study, there would be an increase in current due to methanol oxidation. However, no such current increment in methanol oxidation region is observed in this study. Another vital point to be mentioned here is the Pt–Bi catalysts supported on Vulcan XC 72 R are less susceptible to dissolution when compared with intermetallic PtBi systems [33].

Figure 5 shows the linear sweep voltammograms (LSVs) for methanol oxidation on Pt/C and Pt–Bi/C catalysts in 0.5 M $H_2SO_4$ containing 0.5 M $CH_3OH$ at a sweep rate of 2 mV $s^{-1}$ in the potential range of –650 to 400 $mV_{MSE}$. From the figure, the current densities of MOR on Pt–Bi/C are much lower than those on Pt/C catalyst and also the onset potentials for methanol oxidation peaks on Pt–Bi/C catalysts are shifted to more positive potentials (a considerable shift of 180 mV) as compared to the Pt/C, indicating the negligible/poor oxidation of methanol on Pt–Bi/C catalysts.

It is well established that for methanol oxidation to occur, at least three adjacent Pt sites in a proper geometry is necessary to activate the chemisorption of methanol [35–37]. In this study, Pt–Bi/C catalysts might have disordered surface structure which showed poor activity for methanol oxidation and it is due to the probability of finding three neighbouring Pt atoms on the surface is low.

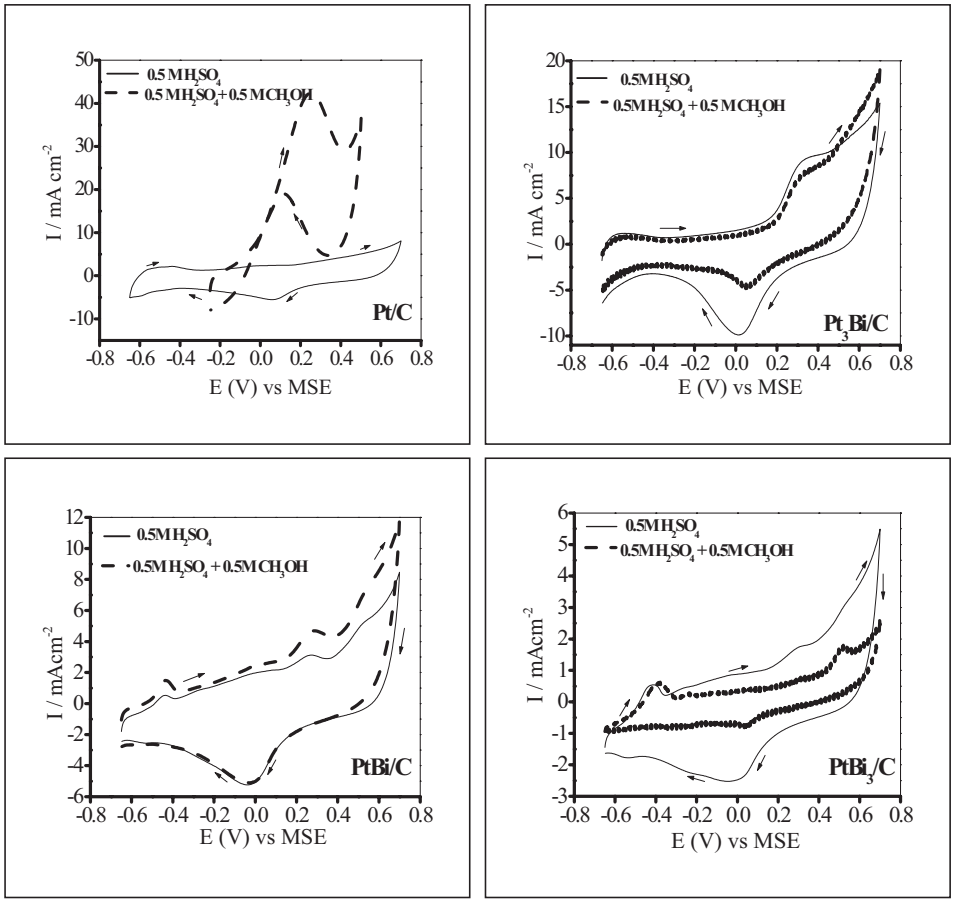


Fig. 4 Cyclic voltammograms of Pt/C and Pt–Bi/C catalysts in 0.5 M $H_2SO_4$ with and without 0.5 M $CH_3OH$ in the potential range of –650 to 700 $mV_{MSE}$ at 50 mV $s^{-1}$ (current densities are normalised to the geometric surface area).

However, a recent work on Pt–Bi/C catalyst by Xia and coworkers [38] showed that PtBi/C catalyst exhibits better catalytic performance than PtRu/C which is known as the best electrocatalyst for methanol oxidation. This observation is contrary to this study and the reason for these different behaviours is due to the difference in the structure of the catalyst. The catalyst synthesised by Xia and coworkers [38], PtBi/C has single and chemically ordered phase, but the catalysts used in the study are disordered as mentioned in Section 3.3. Hence, the structure of the PtBi/C catalyst plays an important factor that decides behaviour of the catalyst.

The high resistance to methanol on Pt–Bi/C catalysts could be due to the distortion of three Pt site requirements by bismuth (third-body effect). It may be stated that the resistance of the adsorbent for an adsorbate is

  

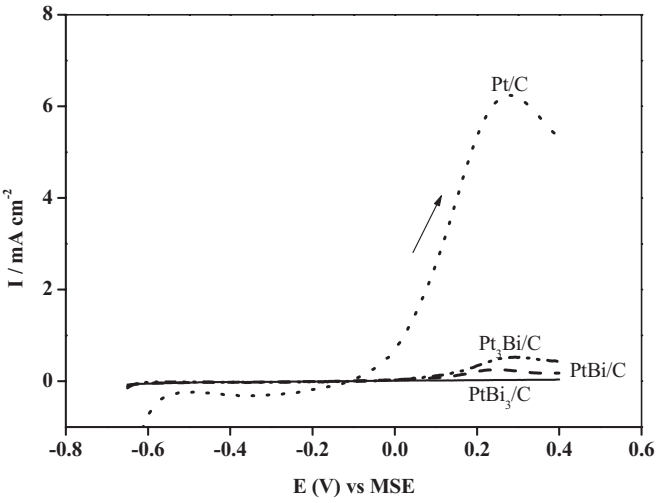


Fig. 5 Polarisation curves of methanol oxidation on Pt/C and Pt–Bi/C catalysts in 0.5 M $H_2SO_4$ containing 0.5 M $CH_3OH$ at 2 mV $s^{-1}$ in the potential range of –250 to 400 $mV_{MSE}$ (current densities are normalised to the geometric surface area).

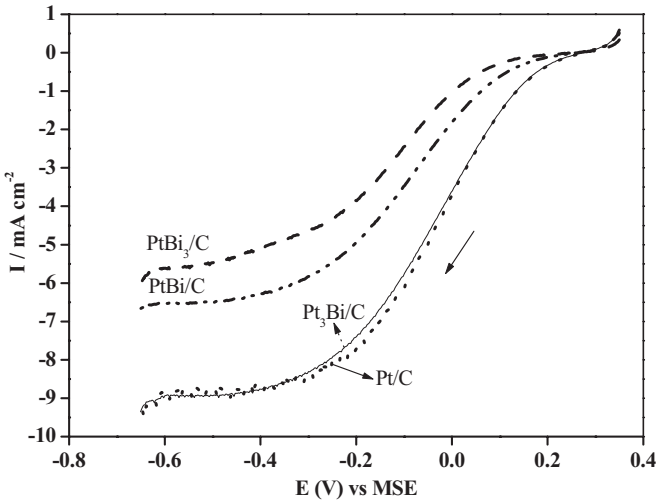


Fig. 6 Polarisation curves for ORR on Pt/C and Pt–Bi/C catalysts in oxygen saturated 0.5 M $H_2SO_4$ at 5 mV $s^{-1}$ in the potential range of 0.35 to –0.65 $V_{MSE}$ at $\omega$ = 2,500 rpm (current densities are normalised to the geometric surface area).

usually determined by the following parameters: (i) low adsorption energy of the adsorbent, (ii) geometric and (iii) electronic effect. While methanol tolerance may largely be due to the third-body effect, the electronic influence exerted by the Bi is not clearly understood. It may be pointed out that the nanoparticles systems under study may not have regular arrangement of Pt and Bi atoms in the lattice and it is difficult at this time to comment on the geometry constraints posed by the nanoparticle assemblies.

### 3.4 ORR Study on Pt/C and Pt–Bi/C Alloy Catalysts

Figure 6 shows the comparison of polarisation curves of ORR activity on Pt/C and $Pt_3Bi$/C, PtBi/C and $PtBi_3$/C catalysts under similar conditions. The LSVs were recorded in the potential region of 350 to –650 $mV_{MSE}$ at a scan rate; 5 mV $s^{-1}$, rotation speed; 2,500 rpm in oxygen-saturated sulphuric acid solution. From the figure, it is seen that the ORR on all catalysts is diffusion controlled at potentials less than –200 $mV_{MSE}$ and under mixed diffusion-kinetic control in the potential region of –200 to 100 $mV_{MSE}$. When the potentials are higher than 100 $mV_{MSE}$, the ORR is under kinetics control (Tafel region). In the Tafel region and mixed control region, it is found that Pt–Bi/C catalysts have higher mass activities for oxygen reduction than that of Pt/C. On $Pt_3Bi$/C catalyst, the oxygen reduction occurs at the same onset potential and overpotential of Pt/C. PtBi/C and $PtBi_3$/C catalysts shift the onset of oxygen reduction to more negative potentials, i.e. about 34 $mV_{MSE}$ (PtBi/C) and 52 $mV_{MSE}$ ($PtBi_3$/C), respectively. The mass activities of the catalysts are in the order: $PtBi_3$/C > PtBi/C > $Pt_3Bi$/C > Pt/C.

The overpotentials of Pt–Bi/C electrodes are similar to that of Pt/C. The cathodic shift of onset potential values for PtBi/C and $PtBi_3$/C catalysts may be due to the Bi-induced formation of oxygenated species that block the Pt active sites.

### 3.5 ORR Study on Pt/C and Pt–Bi/C Alloy Catalysts in the Presence of Methanol

Figure 7 compares LSVs for ORR on Pt/C and Pt–Bi/C catalysts in the potential region of 350 to –650 $mV_{MSE}$ at 5 mV $s^{-1}$ with a rotation speed of 2,500 rpm in oxygen-saturated sulphuric acid solution in the presence of methanol. When comparing the Figures 6 and 7, all catalyst materials except PtBi/C show positive shift in overpotential values in the presence of methanol. Pure Pt/C shows the overpotential loss of 160 $mV_{MSE}$, and onset potential loss of 250 $mV_{MSE}$ to more negative potentials when compared with the potential values of ORR in the absence of methanol and this is due to the competitive reaction between ORR and MOR. In presence of methanol $Pt_3Bi$/C, $PtBi_3$/C catalysts exhibit ~42 and

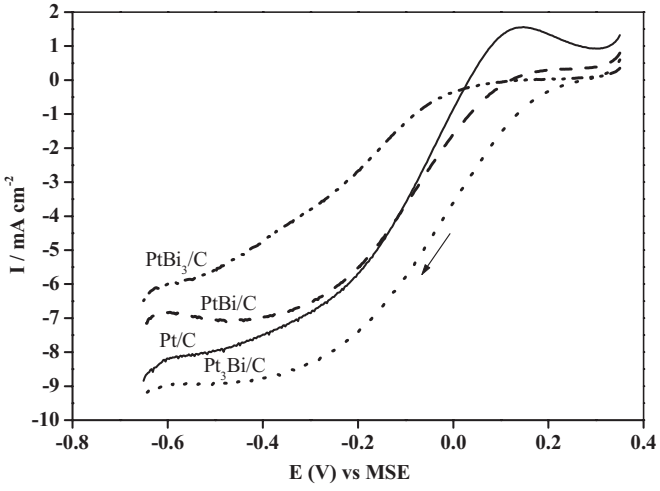


Fig. 7 Polarisation curves for ORR on Pt/C and Pt–Bi/C catalysts at 5 mV $s^{-1}$ in the potential range of 0.35 to –0.65 $V_{MSE}$ at $\omega$ = 2,500 rpm in oxygen saturated 0.5 M $H_2SO_4$ containing 0.5 M $CH_3OH$.

  

85 $mV_{MSE}$ shift in onset potential for ORR from their respective LSVs recorded in 0.5 M $H_2SO_4$.

PtBi/C catalyst does not show any shift in onset and overpotentials in the presence of methanol with respect to those values for ORR without methanol. Hence, PtBi/C catalyst exhibits better methanol-tolerance and ORR activity than the other bismuth-loaded catalysts ($Pt_3Bi/C$ and $PtBi_3/C$). Though methanol tolerance seems to be common with all the Pt–Bi catalysts, there is still an overpotential loss due to the influence of methanol.

High throughput optical screening of Pt-based bimetal catalysts studies reveal that the PtBi/C is one of the combinations which shows the combined effect of higher oxygen reduction activity and methanol-tolerance with acceptable stability that fulfils the requirements of a cathode catalyst [39].

Figure 8 compares the histograms of the mass activity of the Pt/C and Pt–Bi/C catalysts for oxygen reduction in 0.5 M sulphuric acid both in presence and absence of methanol. The mass activity values are collected from the polarisation curves at –100 $mV_{MSE}$. In the Tafel region and the mixed control regions, it is found that the mass activities of Pt–Bi/C catalysts for oxygen reduction are greater than that of pure Pt/C and $PtBi_3/C$ exhibits the highest activity. The mass activities of $Pt_3Bi/C$, PtBi/C and $PtBi_3/C$ for oxygen reduction are varying from 1 to 1.5 times greater than that of Pt/C. All the three Pt–Bi/C catalysts show a small change in the mass activity for oxygen reduction in presence of methanol; however this variation is lower than that of Pt/C.

### 3.6 Electrochemical Characterisation of PtBi/C Catalyst

From the mass activity measurements, it is observed that the Pt–Bi/C catalysts for oxygen reduction activities follow the order $PtBi_3/C$ > PtBi/C > $Pt_3Bi/C$. Though PtBi/C catalyst exhibits intermediate mass activity for oxygen reduction among the other bismuth-loaded catalysts, its ORR activity is not affected in the presence of methanol (as discussed in Section 3.5). This behaviour makes us to study the stability of the PtBi/C catalyst. Hence, the stability of PtBi/C catalyst was studied electrochemically. The CV of the PtBi/C catalyst is recorded in 0.5 M $H_2SO_4$ electrolyte. The PtBi/C catalyst-loaded gold electrode was held at a constant potential of –650 $mV_{MSE}$ in sulphuric acid solution for about 15 min and allowed to cycle in the potential region of –650 to –200 $mV_{MSE}$ and the results are shown in Figure 9.

Figure 9 compares the CVs of the PtBi/C catalyst before labelled as '*a*' and after as '*b*' cathodic polarisation at –650 $mV_{MSE}$. The figure labelled '*b*' clearly shows peaks corresponding to bismuth dissolution and re-deposition are observed during the anodic and cathodic scans, respectively. A peak due to bismuth stripping was observed at –470 $mV_{MSE}$ and the bismuth re-deposition occurs at –580 $mV_{MSE}$ in pure electrolyte.

This observation reveals that bismuth stripped from the surface during the anodic treatment is not completely lost from the surface but re-deposits on the catalyst surface [33, 34] either electrochemically or by spontaneous deposition. This observation was further supported by the scanning electron microscope (SEM) analysis.

### 3.7 SEM Analysis of PtBi/C Catalyst

Experiments were also performed to examine the surface morphology of PtBi/C catalyst before and after the electrochemical treatment using SEM. The PtBi/C catalyst was coated on a carbon paper. SEM image of the sample was recorded and shown in Figure 10a. After electrochemical treatment (as stated Section 3.6), the SEM was again recorded and presented in Figure 10b. The morphology of these two surfaces appears to be different. After the electrochemical treatment, some new deposits are seen on the catalyst surface indicating

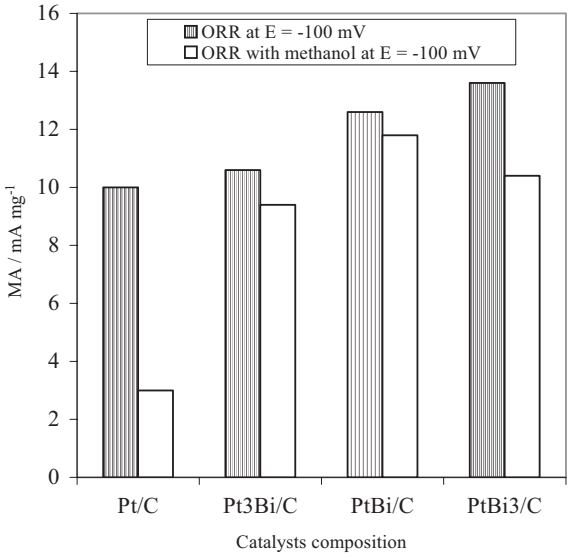


Fig. 8 Histograms showing mass activity of Pt/C and Pt–Bi/C catalysts for ORR in 0.5 M $H_2SO_4$ saturated with oxygen both in the presence and absence of 0.5 M $CH_3OH$.

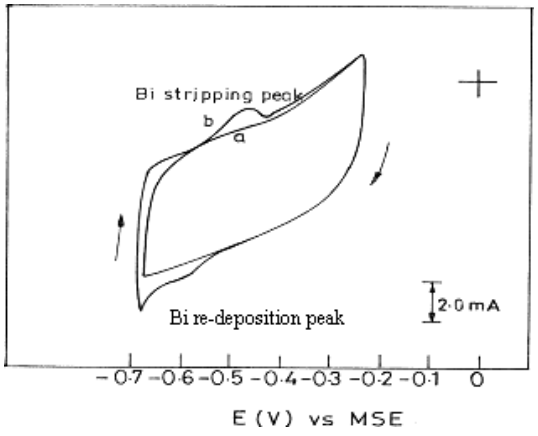


Fig. 9 Cyclic voltammograms of PtBi/C catalyst in the potential region from –650 to –200 mV at 50 mV $s^{-1}$ (a) before and (b) after cathodic polarisation at –650 $mV_{MSE}$.

  

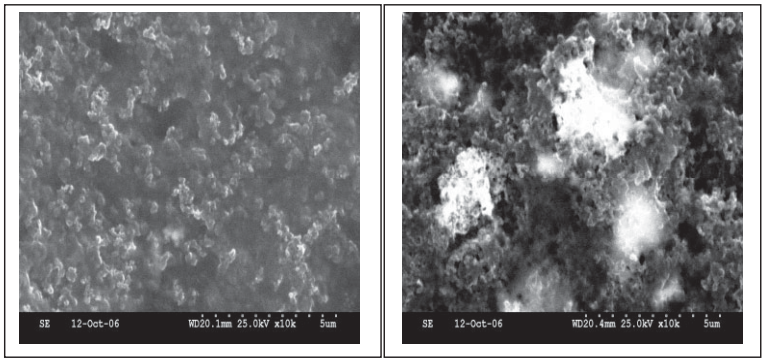


(a) (b)

Fig. 10 The SEM images of a representative PtBi/C catalyst (a) before; and (b) after electrochemical treatment.

that whatever is dissolved during the anodic scan is electrochemically re-deposited in the subsequent cathodic run. Another important property of the bismuth ions in solution is that it can get adsorbed on the surface of the electrode by spontaneous deposition phenomenon. Hence, the bismuth that dissolves is not completely lost from the surface but re-deposits on the surface either through underpotential deposition or spontaneous deposition [40]. The physical nature of such surfaces is intriguing and needs further examination using surface analytical tools.

It is understood from the present investigation that Pt–Bi/C catalysts are inactive for MOR. Though Pt–Bi/C catalysts shift the onset of ORR to more negative potentials, the oxygen reduction current densities are same both in the presence and absence of methanol. This effect may be due to the enrichment (surface segregation effect) of the catalyst surface by platinum due to the leaching of bismuth from the surface. Furthermore, most of Bi lost from the surface at the anodic potentials can be re-deposited during the cathodic scan that renders the surface methanol-resistant.

Thus, Bi presents an interesting system to have a control over the activity of the surface for MOR and ORR. Also, we learned from these observations that in spite of water activation (i.e. favoured Pt–OH formation), ORR still takes place. It is likely that some other factors that may also influence the balance between the ORR activity and methanol-tolerance of the catalyst. Apart from these aspects, utility of catalysts (Pt–Bi/C) with low Bi content, as observed in the case of $Pt_3Bi/C$ in a fuel cell configuration remains to be examined. Considering the factors operative in this kind of studies, the real surface condition responsible for the enhanced ORR activity and methanol tolerance demands a thorough surface analysis. The results published by Xia et al [41] on the behaviour of a methanol-tolerant ORR active $PtBi_2$ phase are also devoid of mechanistic details that can elucidate both methanol tolerance and ORR activity.

## 4 Conclusion

In this study, a series of bimetallic nanostructured catalysts such as $Pt_3Bi/C$, PtBi/C and $PtBi_3/C$ were synthesised by a microemulsion method. The electrochemical study reveals that Pt–Bi/C catalysts exhibit high methanol-tolerance and catalyse ORR to same extents with and without methanol in oxygen-saturated sulphuric acid solutions. The detailed characterisations of the Pt–Bi/C catalysts showed that these catalysts are nanostructured. The XRD patterns of Pt–Bi/C catalysts show the reflections of platinum with *fcc* structure.

Among the various combinations studied, PtBi/C catalyst does not show any change in the onset potential and oxygen reduction current values when methanol is present. The Pt–Bi/C catalysts showed slightly enhanced mass activity by a factor of 1–1.5 for ORR both in the presence and absence of methanol.

It is imperative that these surfaces need to be examined for their ORR activity and as methanol-tolerant cathode catalysts for DMFC. Though these catalysts are suffered by the leaching of bismuth during the anodic scan, the bismuth lost from the surface is readsorbed. Thus the ORR activity of methanol tolerant Pt–Bi/C catalysts could be interpreted due to third-body effect, disordered nature of the catalyst surface, surface composition effect and also due to the relative positioning of Pt and bismuth.

## Acknowledgement

This work was supported by the Council of Scientific and Industrial Research (CSIR), New Delhi, India. We sincerely thank Dr. A. A. M. Prince, Assistant Professor, Department of Chemistry, RKM Vivekananda College, Mylapore, Chennai, Tamil Nadu, India for his valuable suggestions to improve the paper.

## References

[1] J. J. Lingane, *J. Electroanal. Chem.* **1961**, *2*, 296.
[2] L. Zhang, J. Zhang, D. P. Willison, H. Wang, *J. Power Sources* **2006**, *156*, 171.
[3] J. K. Norskov, J. Rossmeisl, A. Logadottir, L. Lindqvist, J. R. Kitchin, T. Bligaard, H. Jonsson, *J. Phy. Chem. B* **2004**, *108*, 17886.
[4] E. L. Santiago, L. C. Varanda, H. M. Villullas, *J. Phys. Chem. C* **2007**, *111*, 3146.
[5] S. C. Zignani, E. Antolini, E. R. Gonzalez, *J. Power Sources* **2008**, *182*, 83.
[6] M. Bron, P. Bogdanoff, S. Fiechter, I. Dorbant, M. Hilgendoff, H. Schulenburg, H. Tributsch, *J. Electroanal. Chem.* **2001**, *500*, 459.
[7] R. W. Reeve, P. A. Christensen, A. J. Dieckenson, A. Hamnett, K. Scott, *Electrochim. Acta* **2000**, *45*, 4237.

  

[8] R. Jiang, D. Chu, *J. Electrochem. Soc.* **2000**, *147*, 4605.
[9] P. Convert, C. Coutanceau, F. Gloaguen, C. Lamy, *J. Appl. Electrochem.* **2001**, *31*, 945.
[10] L. Demarconnay, C. Coutanceau, J.-M. Legèr, *Electrochim. Acta* **2008**, *53*, 3232.
[11] E. Antolini, T. Lopes, E. R. Gonzalez, *J. Alloys Compd.* **2008**, *461*, 253.
[12] S. Koh, M. F. Toney, P. Strasser, *Electrochim. Acta* **2007**, *52*, 2765.
[13] A. K. Shukla, R. K. Raman, N. A. Choudhury, K. R. Priolkar, P. R. Sarode, S. Emura, R. Kumashiro, *J. Electroanal. Chem.* **2004**, *563*, 181.
[14] Y. Wang, P. B. Balbuena, *J. Phys. Chem. B* **2005**, *109*, 18902.
[15] Z. Shi, J. J. Zhang, Z. S. Liu, H. J. Wang, D. P. Wilkinson, *Electrochim. Acta* **2006**, *51*, 1905.
[16] S. Mukerjee, S. Srinivasan, M. P. Soriaga, J. McBreen, *J. Electrochem. Soc.* **1995**, *142*, 1409.
[17] T. Toda, H. Igarashi, H. Uchida, M. Watanabe, *J. Electrochem. Soc.* **1999**, *146*, 3750.
[18] H. Yang, C. Coutanceau, J.-M. Legèr, N. Alonso-Vante, C. Lamy, *J. Electroanal. Chem.* **2005**, *576*, 305.
[19] A. Stassi, C. D'Urso, V. Baglio, A. Di Blasi, V. Antonucci, A. S. Arico, A. M. Castro Luna, A. Bonesi, W. A. Triaca, *J. Appl. Electrochem.* **2006**, *36*, 1143.
[20] R. R. Adzic, N. M. Markovic, A. C. Tripkovic, *Bull. Soc. Chim. Belg.* **1980**, *45*, 399.
[21] R. R. Adzic, in *Advances in Electrochemistry and Electrochemical Engineering*, Vol. 13 (Eds.: H. Gerisher, C. W. Tobias) Wiley-Interscience, New York **1984**, p.159.
[22] N. K. Beck, B. Steiger, G. G. Scherer, A. Wockaun, *Fuel Cells* **2006**, *6*, 26.
[23] T. J. Schmidt, B. N. Grgur, R. J. Behm, N. M. Markovic, P. N. Ross, *Phys. Chem. Chem. Phys.* **2001**, *3*, 3879.
[24] D. Xia, G. Chen, Z. Wang, Z. Zhang, S. Hui, D. Ghosh, H. Wang, *Chem. Mater.* **2006**, *18*, 5746.
[25] L. Demarconnayl, C. Coutanceau, J.-M. Legèr, *Electrochim. Acta* **2008**, *54*, 3232.
[26] C. Jeyabharathi, J. Mathiyarasu, K. L. N. Phani, *J. Appl. Electrochem.* **2009**, *39*, 45.
[27] X. Zhang, K. Y. Chan, *J. Mater. Chem.* **2002**, *12*, 1203.
[28] J. Fang, K. L. Stokes, J. Wiemann, W. Zhou, J. Dai, F. Chen, C. J. O'Conner, *Mater. Sci. Eng., B* **2001**, *83*, 254.
[29] M.-L. Wu, D.-H. Chen, T.-C. Huang, *Colloid Interface Sci.* **2001**, *243*, 102.
[30] A. N. Correia, L. H. Mascaro, S. A. S. Machoda, L. A. Avaca, *Electrochem. Acta* **1997**, *42*, 493.
[31] E. C. Rivera, Z. Gal, A. C. D. Angelo, C. Lind, F. J. Disalvo, H. D. Abruña, *Chem. Phys. Chem.* **2003**, *4*, 193.
[32] M. Oana, R. Hoffmann, H. D. Abruña, F. J. Disalvo, *Surf. Sci.* **2005**, *57*, 41.
[33] D. R. Blasini, D. Rochefort, E. Fachini, L. R. Alden, F. J. Disalvo, C. R. Cabera, H. D. Abruña, *Surf. Sci.* **2006**, *600*, 2670.
[34] A. V. Tripković, K. Dj. Popović, R. M. Stevanović, R. Socha, A. Kowal, *Electrochem. Commun.* **2006**, *8*, 1492.
[35] C. Roychowdhury, F. Matsumoto, P. F. Mutolo, H. D. Abruña, F. J. Disalvo, *Chem. Mater.* **2005**, *17*, 5871.
[36] C. Lamy, A. Lima, V. Lc Rhun, C. Cantaneceau, J.-M. Legèr, *J. Power Sources* **2002**, *105*, 283.
[37] H. A. Gasteiger, N. Markovic, P. N. Ross, Jr., E. J. Cairns, *J. Electrochem. Soc.* **1994**, *141*, 1795.
[38] X. Li, G. Chen, J. Xie, L. Xhang, D. Xia, Z. Wu, *J. Electrochem. Soc.* **2010**, *157*, B580.
[39] J. H. Liu, M. K. Jeon, S. I. Woo, *Appl. Surf. Sci.* **2006**, *252*, 2580.
[40] R. Carbo, R. Albalat, J. Claret, J. M. Feliu, *J. Electroanal. Chem.* **1998**, *446*, 79.
[41] D. Xia, G. Chen, Z. Wang, J. Zhang, S. Hui, D. Ghosh, H. Wang, *Chem. Mater.* **2006**, *18*, 5746.


  